PCCP

Cite this: *Phys. Chem. Chem. Phys.*, 2011, **13**, 5227–5234

www.rsc.org/pccp

**PAPER**



# *In situ* evaluation of anticancer drug methotrexate–DNA interaction using a DNA-electrochemical biosensor and AFM characterization†

**Ana Dora Rodrigues Pontinha,[a] Sônia Maria Alves Jorge,[ab] Ana-Maria Chiorcea Paquim,[a] Victor Constantin Diculescu[a] and Ana Maria Oliveira-Brett*[a]**

***Received 3rd November 2010, Accepted 18th February 2011***
**DOI: 10.1039/c0cp02377a**

An *in situ* evaluation of the dsDNA–methotrexate (MTX) interaction was performed by voltammetry using a DNA-electrochemical biosensor and characterized by atomic force microscopy (AFM) at a highly oriented pyrolytic graphite (HOPG) surface. Electrochemical experiments in incubated solutions showed that the interaction of MTX with dsDNA leads to modifications to the dsDNA structure in a time-dependent manner. The AFM images show reorganization of the DNA self-assembled network on the surface of the HOPG electrode upon binding methotrexate and the formation of a more densely packed and slightly thicker MTX–dsDNA lattice with a large number of aggregates embedded into the network film. The intercalation of MTX between complementary base pairs of dsDNA lead to the increase of purine oxidation peaks due to the unwinding of the dsDNA. The dsDNA-electrochemical biosensor and the purinic homo-polynucleotide single stranded sequences of guanosine and adenosine, poly[G] and poly[A]-electrochemical biosensors, were used to investigate and understand the interaction between MTX and dsDNA.

## 1. Introduction

In recent years increased attention has been focused on the ways in which drugs interact with DNA, with the goal of understanding the toxic as well as chemotherapeutic effects of small molecules used in cancer treatment. There are two main binding modes of small molecules with double-stranded DNA (dsDNA): covalent (chemical modification of DNA bases or sugar constituents) and non-covalent (outer electrostatic binding, groove binding or intercalation). Intercalation results from insertion of a planar aromatic ring system between dsDNA base pairs with concomitant unwinding and lengthening of the DNA helix. In contrast, groove binding involves covalent and non-covalent (electrostatic) interactions that do not perturb the duplex structure to any great extent.

Antimetabolites are a group of drugs that became very important for cancer chemotherapy, being highly effective in targeting and inhibiting the enzymes involved in malignant cells lines.[1] Methotrexate (MTX), N-[4{[2,4-diamino-6-pteridinyl-methyl]-methylamino} benzoyl] glutamic acid (see Scheme 1), is an antimetabolite of folic acid that targets the enzyme dehydrofolate reductase,[2] which plays a supporting but essential role for the synthesis of thymine nucleotide.[3] The inhibition of this enzyme drastically reduces the level of thymidine-monophosphate (dTMP), leading to an increase of the uridine-monophosphate (dUMP) pool, implying significant incorporation of dUMP into DNA.[4–6] These changes are sufficient to overcome the normal excision mechanisms that exclude uracil from DNA with direct effects related to the cytotoxicity of the drug, which in general induces cell death.[7]

MTX is indicated in the treatment of many neoplasms, such as acute leukemia,[8] head and neck cancer,[9] micrometastases of osteosarcoma.[10] It is also used as alternative treatment for psoriasis and rheumatoid arthritis when they are unresponsive to conventional therapies.[11] Besides the benefits observed during treatment with MTX, several side effects such as fetal growth retardation, renal insufficiency, gastrointestinal lesions, marrow suppression, hepatic failure and pancytopenia were

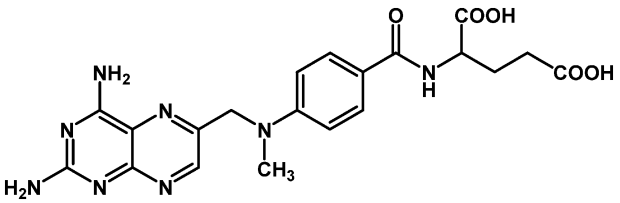


**Scheme 1** Chemical structure of MTX.

[a] *Departamento de Química, Faculdade de Ciências e Tecnologia, Universidade de Coimbra, 3004-535, Coimbra, Portugal. E-mail: brett@ci.uc.pt; Fax: +351-239-835295; Tel: +351-239-835295*
[b] *Departamento de Química e Bioquímica, Instituto de Biociências, UNESP, 18618-000, Botucatu, SP, Brasil*

† This article is part of the special collection on *Interfacial processes and mechanisms* in celebration of John Albery's 75th birthday.

described,[12,13] as well as DNA damage[14,15] and accumulation of potentially lethal 8-hydroxy-2′-deoxyguanosine (8-OHdG) often taking place.[16,17]

Although the DNA damage mechanism of MTX is not clear, apparently involving a cascade of secondary biochemical reactions, there are several studies indicating that MTX is genotoxic[18] resulting in chromosomal/chromatid breaks proving a direct interaction between dsDNA and MTX.[19,20]

The understanding of the mechanism of action of drugs that interact with DNA will explain the differences in reactivity between similar compounds. This knowledge can be used as an important parameter for quantitative structure–activity relationships (QSAR) and/or molecular modelling studies, as a contribution to the design of new structure-specific DNA-binding drugs, and for the possibility of pre-screening the damage they may cause to DNA integrity.

Electrochemical research on DNA is of great relevance to explain many biological mechanisms. The DNA-electrochemical biosensor is a very good model for simulating nucleic acid interaction with cell membranes, potential environmental carcinogenic compounds and for clarifying the mechanisms of action of drugs used as chemotherapeutic agents. An electrochemical sensor for detecting DNA damage consists of an electrode with DNA on its surface. DNA-electrochemical biosensors enable the study of the interaction of DNA immobilized on the electrode surface with analytes in solution, the DNA acting as a promoter between the electrode and the biological molecule under study. Interactions of the surface-confined DNA with a DNA damaging agent are converted, *via* changes in electrochemical properties of the DNA recognition layer, into measurable electrical signals.[21] The electrochemical transduction is dynamic in that the electrode is itself a tuneable charged reagent as well as a detector of all surface phenomena, which greatly enlarges the electrochemical DNA biosensing capabilities. The interaction of a number of substances with DNA has been successfully studied using DNA electrochemical biosensors and the interpretation of the results have contributed to evaluating and predicting DNA interactions, and to the elucidation of the mechanisms by which DNA is damaged by health hazardous compounds, based on their ability to bind to nucleic acids.[21,22]

The advantage of the dsDNA-electrochemical biosensor in studying the mechanisms of anticancer drug–DNA interaction is that it is a clean chemical system, with great sensitivity, offering the possibility to monitor the anticancer drug–DNA interaction under different conditions and allowing pre-concentration onto the sensor surface and *in situ* electrochemical generation of intermediate radical formation and drug metabolites.

A very good understanding of the adsorption and interactions of DNA with solid electrode surfaces is a major concern in DNA-electrochemical biosensor development, and information on the conformation of the adsorbed DNA, as well as the adsorption characteristics, is crucial for biosensor performance.

Extensive studies using atomic force microscopy (AFM) have been undertaken in order to clarify the adsorption behaviour of DNA at carbon electrode surfaces.[21–23] The visualisation of soft molecules, like DNA, weakly bound to the conducting surface of electrochemical transducers is better achieved using magnetic AC mode atomic force microscopy (MAC mode AFM), which enables imaging of the surface morphological structure of adsorbed nucleic acids and understanding of the mechanism of adsorption and the nature of DNA–electrode surface interactions.[22,23]

The development of the DNA-electrochemical biosensor has opened wide perspectives using a particularly sensitive and selective method for the detection of specific interactions. The possibility of foreseeing the damage that these compounds cause to DNA integrity arises from the pre-concentration of either the starting materials or the redox reaction products on the DNA-biosensor surface, thus permitting the electrochemical probing of the presence of short-lived intermediates and of their damage to DNA.[21]

DP voltammetry has been successfully employed for the rapid detection of small perturbations of the double helical structure and DNA oxidative damage,[21,22] due to its high sensitivity and selectivity when compared with other methods reported in the literature, while AFM has given important information concerning DNA structural modifications[21–23] with extraordinary resolution and accuracy.

The use of DNA-electrochemical biosensors for the understanding of DNA interactions with molecules or ions exploits the use of voltammetric techniques for *in situ* generation of reactive intermediates and is a complementary tool for the study of biomolecular interaction mechanisms. Additionally, the interpretation of electrochemical data can contribute to the elucidation of the mechanism by which DNA is oxidatively damaged by such substances, in an approach to the real action scenario that occurs in the living cell, without using animal tests.

In the present paper, a systematic study to elucidate the interaction of MTX with dsDNA was carried out on two different types of carbon electrode, glassy carbon (GCE) using differential pulse (DP) voltammetry and highly oriented pyrolytic graphite (HOPG) using magnetic AC mode atomic force microscopy (MAC mode AFM). The dsDNA-electrochemical biosensor and single stranded purinic homo-polynucleotide poly[G] and poly[A]-electrochemical biosensors, were used to understand *in situ* and in real time the MTX–dsDNA interaction.

## 2. Experimental

### 2.1 Materials and reagents

Methotrexate (MTX), double stranded DNA (dsDNA), polyadenilic (poly[A]) and polyguanilic (poly[G]) acids obtained from Sigma-Aldrich were used without further purification. Stock solutions of 200 μM MTX and 300 μg $mL^{-1}$ dsDNA, poly[A] and poly[G] were prepared in pH 4.5 0.1 M acetate buffer electrolyte using purified water from a Millipore Milli-Q system (conductivity $\leq$ 0.1 μS $cm^{-1}$) and kept at 4 °C.

The pH measurements were carried out with a Crison micropH 2001 pH-meter with an Ingold combined glass electrode. Microvolumes were measured using EP-10 and EP-100 Plus Motorized Microliter Pipettes (Rainin Instrument Co. Inc., Woburn, USA). All experiments were done at room temperature (25 ± 1 °C).

 

### 2.2 Voltammetric parameters and electrochemical cells

Voltammetric experiments were carried out using a μAutolab running with GPES 4.9 software, Eco-Chemie, The Netherlands. Measurements were carried out using a glassy carbon (GCE) ($d$ = 1.5 mm) working electrode, a Pt wire counter electrode, and Ag/AgCl as reference, in a 0.5 mL electrochemical cell. The experimental conditions for differential pulse voltammetry (DPV) were pulse amplitude 50 mV, pulse width 70 ms, scan rate 5 mV $s^{-1}$. The GCE was polished using diamond spray (particle size 3 μm) before each experiment. After polishing, the electrode was rinsed thoroughly with Milli-Q water and placed in supporting electrolyte and various DP voltammograms were recorded until a steady state baseline voltammogram was obtained. This procedure ensured very reproducible experimental results.

### 2.3 Acquisition and presentation of voltammetric data

All the voltammograms presented were background-subtracted and baseline-corrected using the moving average application with a step window of 5 mV included in GPES version 4.9 software. This mathematical treatment improves the visualization and identification of peaks over the baseline without introducing any artefacts, although the peak intensity is, in some cases, reduced (<10%) relative to that of the untreated curve. Nevertheless, this mathematical treatment of the original voltammograms was used in the presentation of all experimental voltammograms for a better and clearer identification of the peaks. The values for peak current presented in all plots were determined from the original untreated voltammograms after subtraction of the baseline.

### 2.4 Atomic force microscopy

HOPG, grade ZYB of 15 × 15 × 2 $mm^3$ dimensions, from Advanced Ceramics Co., USA, was used as a substrate in the MAC mode AFM study. The HOPG was freshly cleaved with adhesive tape prior to each experiment and imaged by AFM in order to establish its cleanliness.

AFM was performed with a PicoSPM controlled by a MAC mode module and interfaced with a PicoScan controller from Agilent Technologies, Tempe, AZ, USA. All the AFM experiments were performed with a CS AFM S scanner with a scan range of 6 μm in $x$–$y$ and 2 μm in $z$, from Agilent Technologies. Silicon type II MAClevers of 225 μm length, 2.8 N $m^{-1}$ spring constants and 60–90 kHz resonant frequencies in air (Agilent Technologies) were used. All AFM images were topographical and were taken with 256 samples per line × 256 lines and scan rates of 0.8–2.0 lines $s^{-1}$. When necessary, MAC mode AFM images were processed by flattening in order to remove the background slope and the contrast and brightness were adjusted.

### 2.5 Sample preparation

MTX–DNA solutions were prepared by incubation at room temperature of dsDNA in pH 4.5 0.1 M acetate buffer with different concentrations of MTX, during different periods of time. Control solutions of dsDNA in pH 4.5 0.1 M acetate buffer were also prepared and stored during the same periods of time in similar conditions to the MTX–DNA incubated solutions.

For the voltammetric experiments, the solutions used were 5 μM MTX, 100 μg $mL^{-1}$ dsDNA and 100 μg $mL^{-1}$ dsDNA incubated with 5 μM MTX. The DP voltammograms were registered after different incubation periods.

For the AFM experiments, the solutions used were 0.5 μM MTX, 10 μg $mL^{-1}$ dsDNA and 10 μg $mL^{-1}$ dsDNA incubated with 0.5 μM MTX for 0 h and 24 h. The MTX, control dsDNA and MTX–DNA modified HOPG surfaces were obtained by depositing 200 μL samples of the appropriate solution of MTX, dsDNA or MTX–DNA onto the freshly cleaved HOPG surface, over a period of 3 min. The excess of solution was gently cleaned with a jet of Millipore Milli-Q water, and the HOPG with adsorbed molecules was then dried in a sterile atmosphere and imaged by MAC mode AFM in air.

The dsDNA-electrochemical biosensors were prepared by successively covering the GCE surface with three drops of 5 μL each of 33 μg $mL^{-1}$ dsDNA solution. After placing each drop on top of the electrode surface, the biosensor was dried under a constant flux of $N_2$. The poly[A]-electrochemical biosensors and the poly[G]-electrochemical biosensors, purinic homo-polynucleotide-electrochemical biosensors, were prepared in the same way as the DNA-electrochemical biosensors.

Incubation with MTX was carried out by keeping the biosensor for different periods of time in a solution containing 100 μM MTX in pH 4.5 0.1 M acetate buffer at room temperature. Before transfer to acetate buffer, the modified electrode was gently washed with deionized water to ensure the removal of unbound MTX.

## 3. Results and discussion

### 3.1 Evaluation of MTX–DNA interaction in incubated solutions

**3.1.1 Voltammetric analysis.** The electrochemical oxidation of MTX at the GCE surface was carried out in a solution of 30 μM MTX in pH 4.5 0.1 M acetate buffer. The DP voltammogram, Fig. 1, showed one main oxidation peak at $E_p$ = +0.77 V corresponding to the oxidation on the MTX diamino-pteridinyl ring.[24,25]

In order to obtain information about the MTX–dsDNA interaction, experiments were performed in incubated solution, as described in section 2.5. DP voltammograms were registered after different incubation time periods of 0 h, 24 h, and 72 h. The GCE surface was always cleaned between consecutive measurements in order to avoid the blocking of the electrode surface by the adsorption of both MTX and dsDNA.

The DP voltammogram obtained in the control dsDNA solution showed two anodic peaks[21] corresponding to the oxidation of the DNA purinic bases, the peak of deoxyguanosine (dGuo), at $E_p$ = +1.00 V, and the peak of deoxyadenosine (dAdo), at $E_p$ = +1.26 V, Fig. 2.

The DP voltammogram obtained immediately after the addition of MTX to the dsDNA solution showed a high MTX oxidation peak at $E_p$ = +0.77 V, followed by the two anodic peaks corresponding to the oxidation of dGuo and

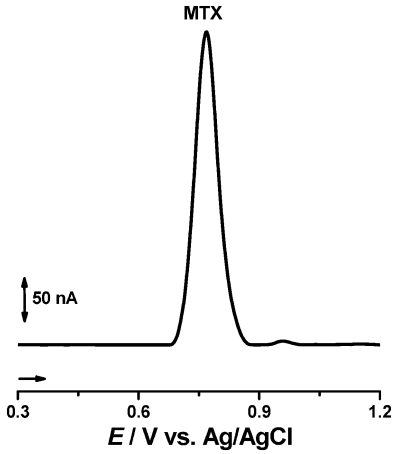


**Fig. 1** DP voltammogram, baseline-corrected, in 30 μM MTX in pH 4.5 0.1 M phosphate buffer.

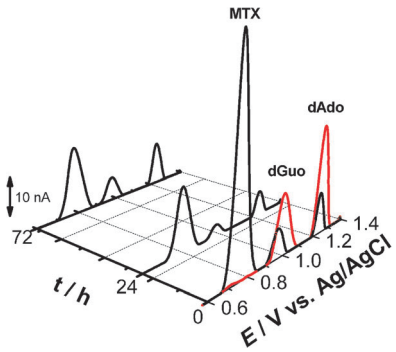


**Fig. 2** DP voltammograms, baseline-corrected, in pH 4.5 0.1 M acetate buffer: ( ▬ ) control 100 μg $mL^{-1}$ dsDNA and (—) solutions of 100 μg $mL^{-1}$ dsDNA with 5 μM MTX incubated for 0 h, 24 h and 72 h.

dAdo, Fig. 2. The results demonstrated that MTX interacts specifically with the dsDNA by intercalation, inducing structural changes in B-DNA, in a time-dependent manner. The reaction in incubated solution was very fast; MTX intercalates into the double-stranded rigid form of DNA inducing DNA condensation, which was confirmed by the diminishing, at 0 h, of the oxidation peaks of dGuo and dAdo, Fig. 2. After 24 h incubation, both the MTX and dsDNA oxidation peaks decreased. For a 72 h incubation time a small increase in the dGuo and dAdo oxidation peak currents was observed whereas the MTX peak current remained constant.

The DP voltammograms showed that structural modifications occur in the DNA double helix in a time-dependent manner upon interaction with MTX and this was also investigated and confirmed by AFM.

**3.1.2 Atomic force microscopy.** The DNA double helix structural modifications that occur in a time-dependent manner upon interaction with MTX in incubated solutions were investigated on a HOPG electrode surface using MAC mode AFM.

For the correct evaluation of the adsorbed molecules and films, an atomically smooth HOPG electrode was used as substrate throughout the AFM study, with less than 0.06 nm of root-mean-square (r.m.s.) roughness for a 1000 × 1000 $nm^2$ surface area. The GC electrode used for the voltammetric characterization was much rougher, with 2.1 nm r.m.s. roughness for the same surface area, and therefore unsuitable for AFM surface characterization.[22,23] Furthermore, the experiments using GC and HOPG electrodes showed similar electrochemical behaviour.

The capacity of MTX to interact and adsorb on carbon electrode surfaces was investigated using MAC mode AFM in air. The MTX modified HOPG was obtained by spontaneous adsorption over a period of 3 min, from a solution of 0.50 μM MTX in 0.1 M pH 4.5 acetate buffer, using the procedure described in section 2.5.

The AFM topographical images of the MTX modified HOPG showed the predisposition of the MTX molecules to adsorb close to each other, forming packed chains with the appearance of nanowires, rod-like and spherical aggregates, Fig. 3A and B. The shape of the MTX assemblies are better visualized in the higher magnification image, Fig. 3C. Many of the short nanowires were approximately 96 nm in length, but sporadically nanowires up to 300 nm long could be also observed. The height and standard deviation of the wires was 0.7 ± 0.1 nm, consistent with the adsorption of a monolayer of MTX molecules, while the globular and rod-like aggregates were slightly higher, with a height of approximately 1.2 nm.

The HOPG surface has a strong impact on the self-assembling proprieties of MTX. HOPG is a polycrystalline material, consisting of individual crystalline domains, which are rotated against each other. The cleaving process of the HOPG electrode with adhesive tape reveals many different atomically flat

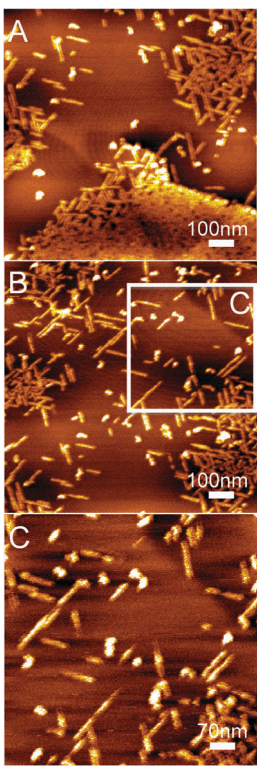


**Fig. 3** AFM images of MTX adsorbed from a solution of 0.5 μM MTX in pH 4.5 0.1 M acetate buffer onto HOPG.

 

terraces on the basal plane of graphite. On flat HOPG terraces, the MTX narrow wire-like structures were oriented mainly along three directions, at 60° and 120° to each other, dictated by the threefold symmetry of the graphite substrate and by the interactions of MTX with the substrate. The formation of these elongated lattices, running in the same direction as the underlying graphite surface, was observed consistently in various independent experiments run under the same experimental conditions.

As observed in the images, the MTX chains were not oriented at a fixed angle relative to the direction of the step edges of the HOPG substrate, indicating that the orientation of the MTX nanowires was not induced by particular surface defects at HOPG step edges, but induced by epitaxial growth on the perfectly flat HOPG terraces, Fig. 3C.

The interaction of MTX with dsDNA was investigated and characterized by MAC mode AFM. In order to have the control adsorption pattern for dsDNA, an AFM study of the spontaneous adsorption from a control solution of 10 μg $mL^{-1}$ dsDNA, Fig. 4A, was undertaken and showed the formation of a thin and incomplete network film with coiled dsDNA molecules.

The MTX–dsDNA modified HOPG surfaces were obtained by spontaneous adsorption from incubated solutions of 10 μg $mL^{-1}$ dsDNA with 0.5 μM MTX, for several periods of time, as described in section 2.5. This procedure led to co-adsorption of MTX–dsDNA, free dsDNA and free MTX molecules on the HOPG substrate.

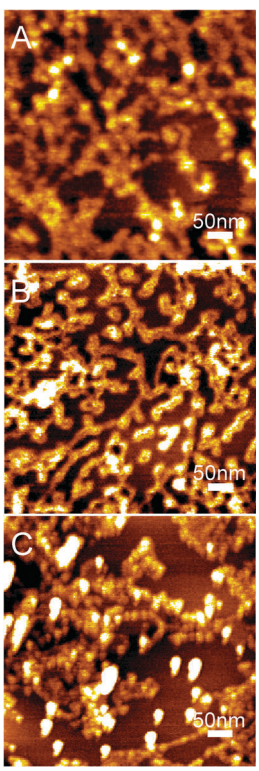


**Fig. 4** AFM images on HOPG: (A) control 10 μg $mL^{-1}$ dsDNA and (B), (C) 10 μg $mL^{-1}$ dsDNA incubated with 0.5 μM MTX for (B) 0 h and (C) 24 h, solutions in pH 4.5 0.1 M acetate buffer.

The MTX–dsDNA layer adsorbed onto HOPG from 0 h incubated solutions of dsDNA with MTX, Fig. 4B, presented a similar pattern of adsorption with the morphology obtained with the dsDNA control solution, Fig. 4A. The MTX–dsDNA network film showed an average height and standard deviation of 0.7 ± 0.2 nm, also consistent with both the height of the control dsDNA layer and the height of a monolayer of adsorbed MTX. However, the epitaxial growth characteristic to the MTX adsorption onto HOPG, Fig. 3, was not observed in the AFM images of MTX–dsDNA, suggesting that the MTX molecules were incorporated by intercalation into the dsDNA.

A different and more complex situation was observed after 24 h incubation time of MTX–dsDNA, Fig. 4C. A reorganization of the dsDNA self-assembled network on the surface of the HOPG electrode was observed in the AFM images, leading to the formation of a more densely packed and slightly thicker MTX–dsDNA lattice, of 1.0 ± 0.2 nm height. Additionally, a large number of 2–6 nm height aggregates were embedded into the network film. After 24 h incubation time of MTX–dsDNA, together with the dsDNA aggregation in the presence of MTX, the decrease of the HOPG surface coverage by MTX–dsDNA layer adsorbed, when compared with the control dsDNA, Fig. 4A, and with the MTX–dsDNA layer adsorbed after 0 h of incubation, Fig. 4B, was also observed.

### 3.2 *In situ* evaluation of methotrexate–DNA interaction

**3.2.1 DNA-electrochemical biosensor.** The evaluation of the MTX–dsDNA interaction in incubated solutions by AFM, Fig. 4, showed the formation of a thin and incomplete network film of co-adsorbed MTX–dsDNA, free dsDNA and free MTX molecules on the HOPG substrate and also the electrode underneath exposed. So, MTX molecules in bulk solution will also diffuse and adsorb non-specifically on the electrode's uncovered regions leading to two different contributions to the electrochemical signal, Fig. 2, one from the simple adsorbed MTX and the other due to the MTX intercalated into dsDNA.

Complete coverage of the electrode surface is necessary and is obtained using the dsDNA-electrochemical biosensor, prepared as described in section 2.5, which avoids the undesired MTX binding to the electrode surface. The dsDNA-electrochemical biosensor response can only arise from the interaction of MTX with dsDNA without any contribution from the diffusion process. The changes occurring to the dsDNA immobilised on the electrode surface during the interaction with MTX were *in situ* and in real time followed by DP voltammetry in the buffer supporting electrolyte solution.

A DP voltammogram of a dsDNA-electrochemical biosensor in pH 4.5 0.1 M acetate buffer, Fig. 5, showed the two anodic peaks[21] corresponding to the oxidation of the DNA purinic bases, the peak of deoxyguanosine (dGuo), at $E_p$ = +1.00 V, and the peak of deoxyadenosine (dAdo), at $E_p$ = +1.26 V, already mentioned, Fig. 2.

The dsDNA-electrochemical biosensor was incubated for 5 min in the MTX solution and then transferred to pH 4.5 0.1 M acetate buffer supporting electrolyte where a DP voltammogram was performed, Fig. 5. The DP voltammogram obtained

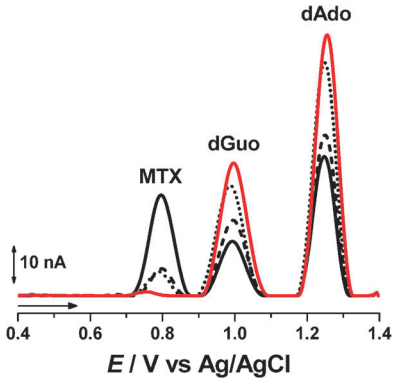


**Fig. 5** DP voltammograms, baseline-corrected, in pH 4.5 0.1 M acetate buffer with dsDNA-electrochemical biosensors ( ▬ ) before and after incubation for (—) 5, (---) 10 and (●●●) 20 min in a solution of 100 μM MTX.

shows the MTX oxidation peak, at $E_p$ = +0.77 V, followed by the peaks due to the oxidation of DNA purinic bases dGuo and dAdo. The binding of MTX molecules to the immobilized dsDNA on the electrode surface led to modifications of the dsDNA-electrochemical biosensor film which are detected by the occurrence of smaller peaks for dGuo and dAdo when compared with the DP voltammograms obtained for the control dsDNA-electrochemical biosensor in buffer.

The experiment was repeated with new dsDNA-electrochemical biosensors, varying the incubation time to 10 and 20 min incubation, Fig. 5. Increasing the incubation time, the MTX oxidation peak decreased reaching a constant current after 10 min incubation. However, the dGuo and dAdo peaks increased in a time-dependent manner.

For short incubation times, the decrease in the DNA oxidation peaks is attributed to the aggregation/condensation of DNA immobilized to the electrode surface because the purine electroactive centres are hidden inside the rigid structure, being unable to reach the GCE surface and consequently unavailable for electrochemical oxidation. This explanation is in agreement with the AFM results from incubated solutions where it was shown that upon incubation with MTX, a more densely packed and slightly thicker MTX–DNA lattice was formed, Fig. 4. Increasing the incubation time, the increase in the DNA oxidation peaks is consistent with unwinding of the immobilized DNA structure exposing the purinic bases to the GCE surface and facilitating the oxidation of the bases dGuo and dAdo.

The DP voltammograms obtained showed that MTX interacts with DNA and can undergo oxidation after binding. For low incubation periods high MTX oxidation peaks were recorded but increasing the incubation time a decrease in the MTX oxidation peak was observed. This effect is attributed to the intercalation of MTX electroactive centres between dsDNA strands being unavailable for electrochemical oxidation.

#### 3.2.2 Purinic homo-polynucleotide-electrochemical biosensors.

In order to obtain more information about the specificity of the MTX–dsDNA interaction and the preferential affinity of MTX to a DNA base, experiments, using purinic homo-polynucleotide single stranded sequence electrochemical biosensors, of guanosine, poly[G], or adenosine, poly[A], electrochemical biosensors, prepared as described in section 2.5, were carried out.

The DP voltammogram of a control poly[G]-electrochemical biosensor in pH 4.5 0.1 M acetate buffer showed only one oxidation peak at +0.98 V, corresponding to dGuo oxidation, Fig. 6. A new poly[G]-electrochemical biosensor was incubated for 5 min in 100 μM MTX, and the peak corresponding to the oxidation of the MTX molecules bound to the immobilized poly[G] strand appeared, Fig. 6. However, the dGuo oxidation peak decreased due to the aggregation of the poly[G] strands immobilized on the GCE surface. Increasing the incubation time to 10 and 20 min, an increase of the dGuo oxidation peak current was observed while the MTX peak current remained constant.

The DP voltammogram of a control poly[A]-electrochemical biosensor in pH 4.5 0.1 M acetate buffer showed only one oxidation peak at +1.26 V, corresponding to dAdo oxidation, Fig. 7. A newly prepared poly[A]-electrochemical biosensor was incubated for 5 min in a 100 μM MTX solution and the DP voltammogram obtained in buffer shows both dAdo and MTX peaks, Fig. 7. The decrease of the dAdo peak was due to the aggregation of poly[A] strands immobilized on the GCE surface. For longer incubation times, of 10 and 20 min, the increase of the dAdo peak is explained by the exposure of the adenine moiety to oxidation on the GCE surface. On the other hand, the decrease of the MTX oxidation peak with increasing the incubation time was observed.

These experiments using purinic homo-polynucleotide single stranded sequences, of poly[G] and poly[A]-electrochemical biosensors, have shown that the interaction of MTX and DNA can occur with both purinic bases. The variation of the MTX oxidation peak with incubation time observed in the case of poly[A]-electrochemical biosensors is an indication of a preferred affinity of MTX to adenine enriched segments.

### 3.3 Interaction between MTX and dsDNA

The interaction mechanism between MTX and dsDNA has to take into consideration that, at pH 4.5, the carboxyl groups of the MTX molecules are negatively charged. The electrostatic repulsion between carboxyl groups of MTX and the negatively

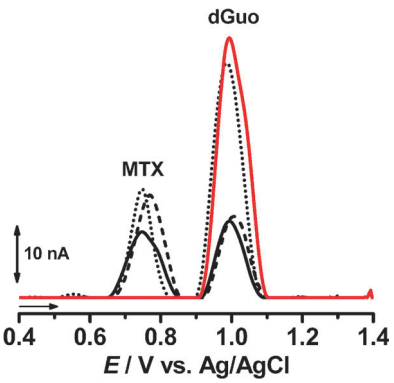


**Fig. 6** DP voltammograms, baseline-corrected, in pH 4.5 0.1 M acetate buffer with poly[G]-electrochemical biosensors ( ▬ ) before and after incubation for (—) 5, (---) 10 and (●●●) 20 min in a solution of 100 μM MTX.

 

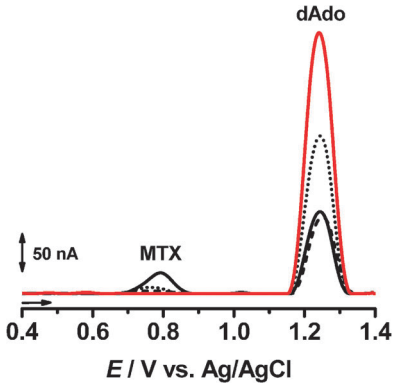


**Fig. 7** DP voltammograms, baseline-corrected, in pH 4.5 0.1 M acetate buffer with poly[A]-electrochemical biosensors ( ▬ ) before and after incubation for (—) 5, (---) 10 and (●●●) 20 min in a solution of 100 μM MTX.

charged phosphate backbone of dsDNA leads to the binding of MTX into the major or minor groove of dsDNA. Therefore, both the electrostatic interaction and the binding of MTX to the dsDNA phosphate backbone[26–28] will impose bending of the dsDNA structure.

The AFM experiments showed the formation of a more densely packed and slightly thicker MTX–dsDNA lattice with a large number of aggregates embedded after adsorption from incubated solutions of MTX and dsDNA, Fig. 4C. The voltammetric measurements showed the decrease of dsDNA oxidation peaks characteristic to the formation of a more rigid structure in which the electroactive centres, dGuo and dAdo, are unable to reach the electrode surface and are consequently unavailable for electrochemical oxidation.

The bending process imposes the kinking of dsDNA,[29] which is actually an inherent DNA response to bending and twisting strains. This alters the original base pair conformation and allows the intercalation of MTX between adjacent dsDNA base pairs.

The intercalation of MTX between dsDNA base pairs was clearly demonstrated by the decrease of the MTX oxidation peak for longer incubation times, Fig. 5. The intercalation induces distortion of the bent dsDNA phosphate backbone allowing better contact between the dsDNA bases and the electrode surface and consequently the increase of the dGuo and dAdo peaks was observed.

The use of purinic homo-polynucleotide-electrochemical biosensors allowed a better understanding of the specificity of the MTX–dsDNA interaction. In the case of poly[G]-electrochemical biosensors, Fig. 6, the MTX oxidation peak did not vary much with incubation time showing that the electroactive centres of MTX are ready to react at the electrode surface, and are therefore always available for electrochemical oxidation. On the contrary, in the case of poly[A]-electrochemical biosensors, Fig. 7, on increasing the incubation time a decrease in the MTX oxidation peak was clearly observed. This allowed us to conclude that the MTX–dsDNA interaction is not selective but the intercalation of MTX electroactive centres showed more affinity for adenine residues which can be explained considering the weakness of the H-bonds that form with adenine (two H-bonds for adenine against three H-bonds for guanine).

The advantage of the use of the dsDNA-electrochemical biosensors is that they clearly showed *in situ* and in real time the changes occurring to the dsDNA immobilised on the electrode surface during the interaction with MTX.

## 4. Conclusion

A systematic study of the DNA–MTX interaction was carried out on two different types of carbon electrode, GCE using DP voltammetry and HOPG using MAC mode AFM. The mechanism of interaction of MTX with dsDNA in incubated solutions was explained taking into consideration the correlation between the redox behaviour and morphological characteristics observed. The AFM images have shown the reorganization of the DNA self-assembled network on the surface of the HOPG electrode after incubation with MTX, and the formation of a more densely packed and thicker MTX–DNA lattice. In agreement with the AFM results, the voltammetric data showed that structural dsDNA modifications occur in a time-dependent manner. The decrease of dsDNA oxidation peaks observed at short incubation times was consistent with a mechanism that involves condensation and formation of more rigid structures due to the intercalation of MTX into DNA strands.

The dsDNA-electrochemical biosensors enabled *in situ* monitoring of both DNA and MTX oxidation peaks, showing that the dsDNA bending process imposes kinking of the strands, which facilitates the intercalation of MTX, causing unwinding of the dsDNA structure and exposing the purinic bases to the GCE surface. The preferred affinity of MTX to adenine-rich segments, which is explained by the weakness of the H-bonds between adenine and thymine, was confirmed using single-stranded purinic homo-polynucleotide biosensors.

The approach described can be used for the understanding of dsDNA interactions with various complex agents and individual chemicals of environmental, food and medical interest. The dsDNA-electrochemical biosensor is a sophisticated tool to study anticancer drug–DNA interaction, and may contribute to drug discovery, providing knowledge about the efficacy of drugs binding to DNA and information on the mechanism of new drug–DNA interaction.

## Acknowledgements

Financial support from Fundação para a Ciência e Tecnologia (FCT), PhD grant SFRH/BD/46026/2008 (A. D. R. Pontinha), Post-Doctoral Grant SFRH/BPD/36110/2007 (V. C. Diculescu), PTDC/QUI/098562/2008 and PTDC/SAU-BEB/104643/2008, POCI 2010 (co-financed by the European Community Fund FEDER), and CEMUC-R (Research Unit 285), and CAPES-Brasil, Post-Doctoral Grant/1211-08-0 (S. M. A. Jorge), is gratefully acknowledged.

## References

1 M. M. Mader and J. R. Henry, *Antimetabolites*, in *Comprehensive Medicinal Chemistry II*, ed. J. B. Taylor and D. J. Triggle, Elsevier, Netherlands, 2007, vol. 7, p. 55.
2 P. T. Ravi Rajagopalan, Z. Zhang, L. McCourt, M. Dwyer, S. J. Benkovic and G. G. Hammes, *Proc. Natl. Acad. Sci. U. S. A.*, 2002, **99**, 13481.
3 M. Krajinovic and A. Moghrabi, *Pharmacogenomics*, 2004, **5**, 819.

4 J. J. Kinahan, M. Often and G. B. Grindey, *Cancer Res.*, 1979, **39**, 3531.
5 M. Goulian, B. Bleile and B. Y. Tseng, *Proc. Natl. Acad. Sci. U. S. A.*, 1980, **77**, 1956.
6 S. H. Berger, D. L. Pittman and M. D. Wyatt, *Biochem. Pharmacol.*, 2008, **76**, 697.
7 D. S. Goodsell, *The Oncologist*, 1999, **4**, 340.
8 G. Gustafsson, K. Schmiegelow, E. Forestier, N. Clausen, A. Glomstein, G. Jonmundsson, L. Mellander, A. Makipernaa, R. Nygaard and U. M. Saarinen-Pihkala, *Leukemia*, 2000, **14**, 2267.
9 C. Vanhaelen, M. Bertrand, R. De Jager and Y. Kenis, *Eur. J. Cancer*, 1979, **15**, 1315.
10 O. Mir, S. Ropert and F. Goldwasser, *Lancet Oncol.*, 2008, **9**, 1198.
11 G. S. Alarcón, *Immunopharmacology*, 2000, **47**, 259.
12 M. E. Lloyd, M. Carr, P. Mcelhatton, G. M. Hall and R. A. Hughes, *QJM*, 1999, **92**, 551.
13 I. J. Cohen, *Med. Hypotheses*, 2007, **68**, 1147.
14 A. K. Saxena, D. Singh and G. Singh, *Biomed. Res.*, 2009, **20**, 28.
15 J. Bartek, C. Lukas and J. Lukas, *Nat. Rev. Mol. Cell Biol.*, 2004, **5**, 792.
16 S. A. Martin, A. McCarthy, L. J. Barber, D. J. Burgess, S. Parry, C. J. Lord and A. Ashworth, *EMBO Mol. Med.*, 2009, **1**, 323.
17 H. Kazutaka, A. Masahiro, H. Yusuke and K. Shosuke, *Photochem. Photobiol.*, 2002, **76**, 467.
18 S. Padmanabhan, D. N. Tripathi, A. Vikram, P. Ramarao and G. B. Jena, *Mutat. Res., Genet. Toxicol. Environ. Mutagen.*, 2009, **673**, 43.
19 C. Keshava, N. Keshava, W.-Z. Whong, J. Nath and T. M. Ong, *Mutat. Res., Fundam. Mol. Mech. Mutagen.*, 1998, **397**, 221.
20 A. Lorico, G. Toffoli, M. Boiocchi, E. Erba, M. Broggini, G. Rappa and M. D'Incalci, *Cancer Res.*, 1988, **48**, 2036.
21 A. M. Oliveira-Brett, V. Diculescu, A. M. Chiorcea-Paquim and S. H. P. Serrano, in *Comprehensive Analytical Chemistry (CAC)*, ed. Salvador Alegret and Arben Merkoçi, Electrochemical Sensor analysis (ECSA). Section F. Biosensors, 2007, vol 49, p. 413.
22 O. Corduneanu, A.-M. Chiorcea-Paquim, V. Diculescu, S. M. Fiuza, M. P. M. Marques and A. M. Oliveira-Brett, *Anal. Chem.*, 2010, **82**, 1245.
23 A. M. Oliveira-Brett and A. M. Chiorcea-Paquim, *Langmuir*, 2003, **19**, 3830.
24 F. Palmisano, T. R. I. Cataldi and P. G. Zambonin, *J. Chromatogr., Biomed. Appl.*, 1985, **344**, 249.
25 L. Genestier, R. Paillot, L. Quemeneur, K. Izeradjene and J.-P. Revillard, *Immunopharmacology*, 2000, **47**, 247.
26 J. Curuksu, M. Zacharias, R. Lavery and K. Zakrzewska, *Nucleic Acids Res.*, 2009, **37**, 3766.
27 A. A. Salzberg and P. C. Dedon, *Biochemistry*, 2000, **39**, 7605.
28 A. M. Ababneh, Z. Q. Ababneh and C. C. Large, *J. Theor. Biol.*, 2008, **252**, 742.
29 L. J. Maher, *Structure*, 2006, **14**, 1479.


 